Computers and Chemical Engineering 177 (2023) 108318

Contents lists available at ScienceDirect

Computers and Chemical Engineering

journal homepage: www.elsevier.com/locate/cace

Analytical solutions for the modeling, optimization, and control of microwave-assisted freeze drying

Prakitr Srisuma [a,b,c], George Barbastathis [a,c], Richard D. Braatz [b,c,*]

[a] Department of Mechanical Engineering, Massachusetts Institute of Technology, Cambridge, MA 02139, United States of America
[b] Department of Chemical Engineering, Massachusetts Institute of Technology, Cambridge, MA 02139, United States of America
[c] Center for Computational Science and Engineering, Massachusetts Institute of Technology, Cambridge, MA 02139, United States of America

ARTICLE INFO

Dataset link: https://github.com/PrakitrSrisuma/Microwave-Lyophilization

Keywords:
Lyophilization
Freeze drying
Microwave-assisted freeze drying
Hybrid freeze drying
Biopharmaceutical manufacturing

ABSTRACT

Freeze drying, aka lyophilization, is a process by which a pharmaceutical product is dried via sublimation under vacuum. An alternative to the conventional process is microwave-assisted freeze drying, which relies on microwave irradiation for drying the product, offering a reduction in the drying time by 70%–80%. This article derives exact and approximate analytical solutions to a mechanistic model for conventional, microwave-assisted, and hybrid freeze drying. The exact solution serves as a reference solution for validating numerical or approximate results due to its highest accuracy up to machine precision. The approximate solution can be computed about 4-fold faster than the numerical solutions and 200-fold faster than the exact solution with the maximum error of less than 1%, which is highly computationally efficient and accurate. Applications of the analytical solutions are demonstrated in the context of parameter estimation, optimal control, and parameter space analysis.

1. Introduction

Freeze drying, aka lyophilization, is a crucial process in biopharmaceutical manufacturing by which a product is dried (or dehydrated) via sublimation under vacuum (Fissore et al., 2018; Park et al., 2021). To achieve sublimation, the process is carried out at low temperature compared to typical dehydration and drying techniques, and hence freeze drying is better at preserving the quality and structure of heat-sensitive materials, e.g., pharmaceutical products (Barresi et al., 2009). This freeze-drying technique plays an important role in biotherapeutics (Fissore et al., 2018), including applications related to global pandemics such as COVID-19 (Hammerling et al., 2021).

Freeze drying consists of three stages, namely (1) freezing, (2) primary drying, and (3) secondary drying. During freezing, the product and liquid solvent (usually water) are frozen at a very low temperature (Fissore et al., 2018; Bano et al., 2020). In this stage, the free water becomes ice crystals, whereas the bound water retains its noncrystalline state while being bound to the product molecules (Fissore et al., 2018). In primary drying, the frozen product and solvent are heated under sufficiently low pressure and temperature that the ice crystals sublimate (Pisano et al., 2010). In secondary drying, the product is heated further at higher temperature to remove much of the bound water via desorption (Velardi and Barresi, 2008; Gitter et al., 2019).

Primary drying is recognized as the most time-consuming, hazardous, and expensive stage, and so is the main target for improvement and optimization (Velardi and Barresi, 2008; Pisano et al., 2010). In conventional freeze drying (CFD), the product is heated via a heating shelf located under the drying chamber or vial during the drying stages (Pisano et al., 2010; Fissore et al., 2018). To accelerate the drying process, microwave-assisted freeze drying (MFD), which relies on microwave irradiation, was studied and developed (Walters et al., 2014; Gitter et al., 2019). It was shown via both simulations and experiments that MFD can significantly reduce the drying time during primary drying by 70%–80% while still preserving the quality of the product (Gitter et al., 2018; Bhambhani et al., 2021; Park et al., 2021). Hybrid freeze drying (HFD), which combines both CFD and MFD heating techniques, can further decrease the drying time (Park et al., 2021).

Mathematical models of freeze drying are valuable for guiding the design, optimization, and control of the freeze-drying process (Pisano et al., 2010; Fissore et al., 2015; Bano et al., 2020). Over the past few decades, mechanistic modeling of CFD has become well established (see examples and discussions in Litchfield and Liapis, 1979; Mascarenhas et al., 1997; Pikal et al., 2005; Hottot et al., 2006; Velardi and Barresi, 2008; Pisano et al., 2010; Chen et al., 2015; Fissore et al., 2015; Scutellà et al., 2017; Bano et al., 2020). Mechanistic modeling of MFD

* Corresponding author at: Department of Chemical Engineering, Massachusetts Institute of Technology, Cambridge, MA 02139, United States of America.
E-mail address: braatz@mit.edu (R.D. Braatz).

https://doi.org/10.1016/j.compchemeng.2023.108318
Received 18 March 2023; Received in revised form 21 May 2023; Accepted 25 May 2023
Available online 1 June 2023

is not as mature as that of CFD; only a few mechanistic models are available (Witkiewicz and Nastaj, 2010; Wang et al., 2020; Park et al., 2021). A mechanistic model for HFD can be constructed by merging the mechanistic models for CFD and MFD (Park et al., 2021).

The aforementioned mechanistic models are usually written as partial differential equations (PDEs) describing heat and mass transfer in freeze drying, so most previous research heavily relied on numerical solutions, e.g., the finite element method (Mascarenhas et al., 1997; Hottot et al., 2006; Chen et al., 2015) and the finite volume method (Park et al., 2021). Numerical solutions are useful in applications where the model equations are so complicated that analytical solutions cannot be derived. A drawback is that numerical solutions do not explicitly reveal the relationships between model parameters and solutions. The high computational cost is also a limitation for some applications, such as in model-based optimal control (Klepzig et al., 2020). Analytical solutions, on the other hand, are generally more accurate and easier to compute. In addition, analytical solutions allow the connections between model parameters and solutions to be interpreted clearly, which is beneficial in understanding the physics of the system and in engineering design.

This article derives analytical solutions to the established mechanistic model of conventional, microwave-assisted, and hybrid freeze drying during primary drying. The exact analytical solution is obtained by using the superposition principle, separation of variables, and Duhamel's theorem. The approximate analytical solution is derived using the heat-balance integral, which for this system is equivalent to the integral method. The analytical solutions are compared with the numerical solutions based on the finite difference and finite element methods in terms of accuracy and computational performance. Applications of the analytical solutions are demonstrated for parameter estimation, optimal control, and parameter space analysis.

This article is organized as follows. Section 2 describes the mechanistic model for simulating primary drying. Section 3 derives the exact and approximate analytical solutions to the mechanistic model. Section 4 briefly describes techniques used to generate numerical solutions for comparing with the analytical solutions. Section 5 discusses the accuracy and computational performance of the obtained solutions, and demonstrates their applications. Finally, Section 6 summarizes the study and suggests some future directions.

2. Model formulation and description

This section describes the mechanistic model for CFD, MFD, and HFD used in this study.

2.1. Mathematical model

The mechanistic model used in this work is based primarily on the simplified model of Park et al. (2021) (Fig. 1). The model is formulated in the rectangular coordinate system by considering one spatial dimension (x) and time (t). The model consists of two main parts. The first part describes the spatiotemporal evolution of the temperature in the frozen region before sublimation starts. During this period, it is assumed that there is no phase change in the system, with the supplied heat increasing the temperature of the frozen region. The second part describes the evolution of sublimation to predict the drying time by assuming that the supplied heat is used for sublimation only. We denote the first part of the model as the heating stage for $0 \le t < t_m$ and the second part of the model as the sublimation stage for $t \ge t_m$, where t_m is the time when sublimation begins.

During the heating stage, the energy conservation equation for the frozen region is

$$\rho C_P \frac{\partial T}{\partial t} = k \frac{\partial^2 T}{\partial x^2} + H_v, \qquad 0 < x < L, \qquad 0 < t < t_m, \tag{1}$$

where $T(x,t)$ is the temperature, H_v is the microwave irradiation term, ρ is the frozen material density, k is the frozen material thermal conductivity, C_P is the frozen material heat capacity, and L is the length/height of the frozen material. In terms of the thermal diffusivity $\alpha = k/(\rho C_P)$, (1) becomes

$$\frac{1}{\alpha}\frac{\partial T}{\partial t} = \frac{\partial^2 T}{\partial x^2} + \frac{H_v}{k}. \tag{2}$$

During this heating stage, the microwave irradiation term H_v can be approximated by

$$H_v = H_w p_{bw}, \tag{3}$$

where H_w is the volumetric heat generation by the microwave affecting the water and p_{bw} is the portion of the bound water at the initial state. At the bottom surface, the frozen material is heated by the bottom shelf, and thus the boundary condition follows Newton's law of cooling

$$-k\frac{\partial T}{\partial x}(L,t) = h(T(L,t) - T_b(t)), \qquad 0 < t < t_m, \tag{4}$$

where h is the heat transfer coefficient at the bottom (sometimes known as K_v in previous literature) and $T_b(t)$ is the bottom shelf temperature. The shelf temperature increases linearly as a function of time, which results in

$$T_b(t) = rt + T_{b0}, \tag{5}$$

where T_{b0} is the initial shelf temperature and r is the ramp-up rate. At the top boundary, heat transfer is negligible compared to the bottom shelf, and hence the boundary condition is

$$k\frac{\partial T}{\partial x}(0,t) = 0, \qquad 0 < t < t_m. \tag{6}$$

The initial temperature of the frozen region is uniform at T_0,

$$T(x,0) = T_0, \qquad 0 \le x \le L. \tag{7}$$

During this stage, there is no phase change (sublimation), thus no moving interface. In the system, the temperature is highest at the bottom surface of the frozen material following the temperature gradient. When the temperature at the top of the vial reaches the sublimation temperature, sublimation starts. Therefore, we specify the criterion for switching from the heating stage to the sublimation stage as

$$T(0,t_m) = T_m, \tag{8}$$

where T_m is the sublimation temperature.

During the sublimation stage, the evolution of the moving interface (sublimating interface) can be described by the energy balance

$$\frac{ds}{dt} = \frac{H_b(t) + H_v L}{(\rho - \rho_a)\Delta H_{\text{sub}} p_{\text{ice}}}, \qquad t > t_m, \tag{9}$$

where $s(t)$ is the position of the moving interface, $H_b(t)$ is the heat transfer from the bottom shelf, H_v is the microwave irradiation, ρ_a is the density of the dried region, ΔH_{sub} is the latent heat of sublimation, and p_{ice} is the portion of the ice at the initial state. The microwave irradiation H_v during sublimation is slightly different from that of the heating stage, which can be approximated by

$$H_v = H_w p_w, \tag{10}$$

where H_w is as defined in (3) and p_w is the parameter describing water-related portions during sublimation. For the bottom shelf,

$$H_b(t) = h(T_b(t) - T_m), \tag{11}$$

where the temperature of the vial is approximately constant at T_m, the sublimation point, during sublimation. The initial condition for the position of the moving interface for the sublimation stage is

$$s(t_m) = 0. \tag{12}$$

The above simplified model considers two important heat sources: (1) a heating shelf and (2) microwave irradiation. Other heat transfer mechanisms discussed in the literature are thermal radiation and convective heat transfer. The former can be neglected for vials positioned

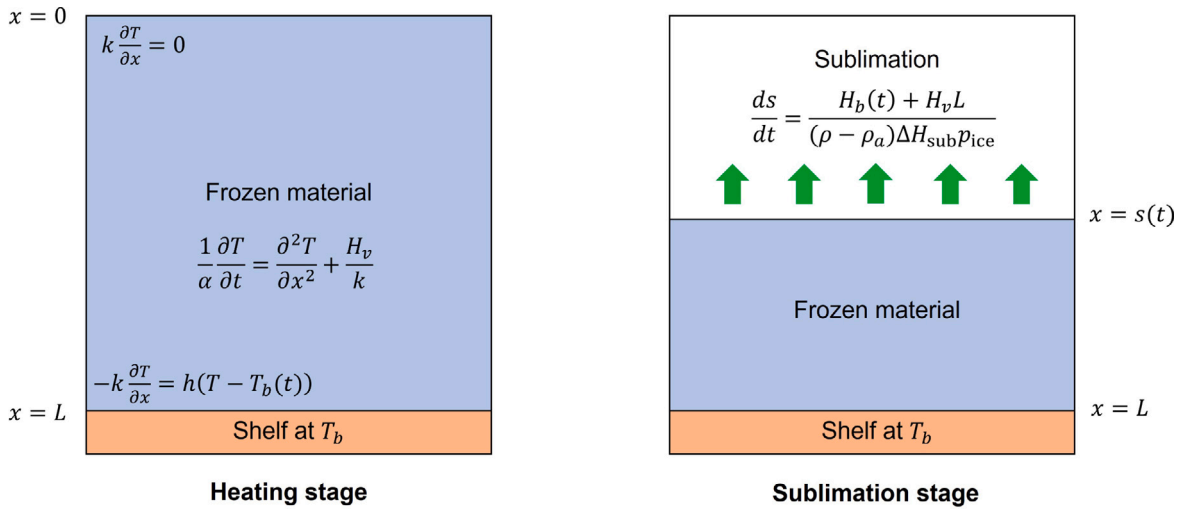

Fig. 1. Schematic diagram of the freeze-drying process.

at the center of the shelf as they are shielded from the surrounding environment, but has significant effect on the drying time for vials at the edge (around 20%–30%) (Velardi and Barresi, 2008). For the latter, a detailed study showed an error of only 5% when neglecting convective effects in conventional freeze drying (Pikal et al., 2016). Although both radiation and convective effects could vary among different experimental setups, these contributions can reasonably be taken into account by adjusting the heat transfer coefficient h defined in (4) as suggested by Pikal et al. (2005).

2.2. Nondimensionalization

Define the dimensionless variables

$$\Theta = \frac{T - T_{b0}}{T_{\text{m}} - T_{b0}}, \tag{13}$$

$$\xi = \frac{x}{L}, \tag{14}$$

$$\eta = \frac{s}{L}, \tag{15}$$

$$\tau = \frac{\alpha t}{L^2}, \tag{16}$$

$$\nu = \frac{hL}{k}, \tag{17}$$

$$\sigma = \frac{rL^2}{\alpha(T_m - T_{b0})}, \tag{18}$$

$$\lambda = \frac{H_w p_{bw} L^2}{k(T_m - T_{b0})}, \tag{19}$$

$$\kappa = \frac{L(H_b + H_w p_w L)}{\alpha \Delta H_{\text{sub}} p_{\text{ice}}(\rho - \rho_a)}, \tag{20}$$

where ν is the Biot number (Bird et al., 2002). Prior to sublimation, the equation of energy for the frozen region (2) in dimensionless form is

$$\frac{\partial \Theta}{\partial \tau} = \frac{\partial^2 \Theta}{\partial \xi^2} + \lambda, \qquad 0 < \xi < 1, \qquad 0 < \tau < \tau_m, \tag{21}$$

where τ_m is the dimensionless time defined at t_m. The boundary condition (4) becomes

$$-\frac{\partial \Theta}{\partial \xi}(1, \tau) = \nu(\Theta(1, \tau) - \sigma\tau), \qquad 0 < \tau < \tau_m. \tag{22}$$

The boundary condition (6) is

$$\frac{\partial \Theta}{\partial \xi}(0, \tau) = 0, \qquad 0 < \tau < \tau_m. \tag{23}$$

The initial temperature is

$$\Theta(\xi, 0) = \Theta_0, \qquad 0 \le \xi \le 1. \tag{24}$$

The criterion for switching from the heating stage to the sublimation stage is

$$\Theta(0, \tau_m) = 1. \tag{25}$$

During sublimation, the evolution of the moving interface (9) becomes

$$\frac{d\eta}{d\tau} = \kappa, \qquad \tau > \tau_m, \tag{26}$$

with the initial condition

$$\eta(\tau_m) = 0. \tag{27}$$

As κ is a function of time, it is useful to rewrite the equation more explicitly

$$\frac{d\eta}{d\tau} = \kappa_1 \tau + \kappa_2, \qquad \tau > \tau_m, \tag{28}$$

where

$$\kappa_1 = \frac{rhL^3}{\alpha^2 \Delta H_{\text{sub}} p_{\text{ice}}(\rho - \rho_a)}, \tag{29}$$

$$\kappa_2 = \frac{L(h(T_{b0} - T_m) + H_w p_w L)}{\alpha \Delta H_{\text{sub}} p_{\text{ice}}(\rho - \rho_a)}. \tag{30}$$

3. Derivation of the analytical solutions

This section derives analytical solutions to the freeze-drying model in Section 2, including the exact and approximate solutions.

3.1. Exact solution for the heating stage

First, the nondimensionalized energy balance during the heating stage is defined as Problem A:

$$\frac{\partial \Theta_{\text{A}}}{\partial \tau} = \frac{\partial^2 \Theta_{\text{A}}}{\partial \xi^2} + \lambda, \qquad 0 < \xi < 1, \qquad 0 < \tau < \tau_m, \tag{31}$$

$$\frac{\partial \Theta_{\text{A}}}{\partial \xi} = 0, \qquad \xi = 0, \qquad 0 < \tau < \tau_m, \tag{32}$$

$$\frac{\partial \Theta_{\text{A}}}{\partial \xi} = -\nu(\Theta_{\text{A}} - \sigma\tau), \qquad \xi = 1, \qquad 0 < \tau < \tau_m, \tag{33}$$

$$\Theta_{\text{A}} = \Theta_0, \qquad 0 \le \xi \le 1, \qquad \tau = 0, \tag{34}$$

where Θ_{A} denotes the solution to Problem A, which is the original problem. This nonhomogeneous PDE with a time-varying boundary condition is solved by the *principle of superposition*, which divides the original problem into a number of simpler subproblems such that the solution to the original problem is the superposition (sum) of the

solutions to all of the subproblems; a comprehensive explanation and examples of the superposition principle are given in Mills (1995).

Applying the principle of superposition to Problem A divides this problem into two subproblems, namely Problems B and C. Problem B is defined as

$$\frac{\partial \Theta_B}{\partial \tau} = \frac{\partial^2 \Theta_B}{\partial \xi^2} + \lambda, \qquad 0 < \xi < 1, \qquad 0 < \tau < \tau_m, \tag{35}$$

$$\frac{\partial \Theta_B}{\partial \xi} = 0, \qquad \xi = 0, \qquad 0 < \tau < \tau_m, \tag{36}$$

$$\frac{\partial \Theta_B}{\partial \xi} = -\nu \Theta_B, \qquad \xi = 1, \qquad 0 < \tau < \tau_m, \tag{37}$$

$$\Theta_B = \Theta_0, \qquad 0 \le \xi \le 1, \qquad \tau = 0, \tag{38}$$

where Θ_B denotes the solution to Problem B. The only difference between Problems A and B is that the original boundary condition (33) in Problem A is time-dependent, whereas the boundary condition (37) in Problem B is not.

Problem C is defined as

$$\frac{\partial \Theta_C}{\partial \tau} = \frac{\partial^2 \Theta_C}{\partial \xi^2}, \qquad 0 < \xi < 1, \qquad 0 < \tau < \tau_m, \tag{39}$$

$$\frac{\partial \Theta_C}{\partial \xi} = 0, \qquad \xi = 0, \qquad 0 < \tau < \tau_m, \tag{40}$$

$$\frac{\partial \Theta_C}{\partial \xi} = -\nu(\Theta_C - \sigma\tau), \qquad \xi = 1, \qquad 0 < \tau < \tau_m, \tag{41}$$

$$\Theta_C = 0, \qquad 0 \le \xi \le 1, \qquad \tau = 0, \tag{42}$$

where Θ_C denotes the solution to Problem C. Problem C has no heat generation (λ) in (39), and the initial condition (42) is 0 rather than Θ_0.

The superposition of the solutions to Problems B and C is the solution to Problem A,

$$\Theta_A = \Theta_B + \Theta_C. \tag{43}$$

Instead of solving Problem A directly, Problems B and C are solved, and the principle of superposition is used to obtain the solution to Problem A. At this stage, Problem C is simplified enough to be solved analytically, whereas Problem B can be further simplified, i.e., by applying another superposition.

Applying the superposition principle to Problem B results in two more subproblems, labeled as Problems B1 and B2. Problem B1 is

$$\frac{d^2 \Theta_{B1}}{d\xi^2} = -\lambda, \qquad 0 < \xi < 1, \tag{44}$$

$$\frac{d \Theta_{B1}}{d\xi} = 0, \qquad \xi = 0, \tag{45}$$

$$\frac{d \Theta_{B1}}{d\xi} = -\nu \Theta_{B1}, \qquad \xi = 1, \tag{46}$$

where Θ_{B1} denotes the solution to Problem B1. Problem B1 is a steady-state problem that can be solved straightforwardly.

Problem B2 is defined as

$$\frac{\partial \Theta_{B2}}{\partial \tau} = \frac{\partial^2 \Theta_{B2}}{\partial \xi^2}, \qquad 0 < \xi < 1, \qquad 0 < \tau < \tau_m, \tag{47}$$

$$\frac{\partial \Theta_{B2}}{\partial \xi} = 0, \qquad \xi = 0, \qquad 0 < \tau < \tau_m, \tag{48}$$

$$\frac{\partial \Theta_{B2}}{\partial \xi} = -\nu \Theta_{B2}, \qquad \xi = 1, \qquad 0 < \tau < \tau_m, \tag{49}$$

$$\Theta_{B2} = \Theta_0 - \Theta_{B1}, \qquad 0 \le \xi \le 1, \qquad \tau = 0, \tag{50}$$

where Θ_{B2} denotes the solution to Problem B2. Problem B2 is similar to Problem B except that (47) does not contain a generation term, and the initial condition (50) is shifted by the solution to Problem B1 (Θ_{B1}).

With this formulation, the superposition of the solutions to Problems B1 and B2 is the solution to Problem B,

$$\Theta_B = \Theta_{B1} + \Theta_{B2}. \tag{51}$$

Therefore, we can solve Problems B1 and B2 instead of Problem B, and then apply the superposition principle to obtain the solution to Problem B.

With all the subproblems established, the next sections concern solving these subproblems.

3.1.1. Solution to Problem B1

Integrating (44) twice results in

$$\Theta_{B1} = -\frac{\lambda \xi^2}{2} + K_1 \xi + K_2, \tag{52}$$

where K_1 and K_2 are the constants of integration. Differentiating (52) gives

$$\frac{d\Theta_{B1}}{d\xi} = -\lambda \xi + K_1. \tag{53}$$

The constants K_1 and K_2 can be determined using (45), (46), (52), and (53), which leads to

$$K_1 = 0, \tag{54}$$

$$K_2 = \lambda\left(\frac{1}{\nu} + \frac{1}{2}\right). \tag{55}$$

Consequently, the solution to Problem B1 is

$$\Theta_{B1} = -\frac{\lambda \xi^2}{2} + \lambda\left(\frac{1}{\nu} + \frac{1}{2}\right). \tag{56}$$

3.1.2. Solution to Problem B2

Before solving Problem B2, the initial condition (50) is rewritten by using the information from (56), leading to

$$\Theta_{B2} = \Theta_0 + \frac{\lambda \xi^2}{2} - \lambda\left(\frac{1}{\nu} + \frac{1}{2}\right), \qquad 0 \le \xi \le 1, \qquad \tau = 0. \tag{57}$$

To solve Problem B2, the method of separation of variables is employed (Mills, 1995). This technique assumes that the solution Θ_{B2} satisfies

$$\Theta_{B2} = F(\tau)G(\xi). \tag{58}$$

Substituting (58) into (47), with some rearranging, yields

$$\frac{1}{F}\frac{dF}{d\tau} = \frac{1}{G}\frac{d^2G}{d\xi^2}, \tag{59}$$

where the partial derivatives are replaced by the total derivatives because $F = F(\tau)$ and $G = G(\xi)$. The left-hand side of (59) is a function of τ, whereas the right-hand side is a function of ξ only. To make this equality hold, both sides must be equal to a constant denoted as $-\beta^2$ in this case. The constant is chosen to be a negative number in order to satisfy the boundary conditions. As a result, (59) can be divided into two ordinary differential equations (ODEs):

$$\frac{1}{F}\frac{dF}{d\tau} = -\beta^2, \tag{60}$$

$$\frac{1}{G}\frac{d^2G}{d\xi^2} = -\beta^2. \tag{61}$$

Both (60) and (61) are integrated to obtain the expressions of F and G, which are substituted into (58) to give

$$\Theta_{B2} = e^{-\beta^2\tau}(K_3 \cos\beta\xi + K_4 \sin\beta\xi). \tag{62}$$

Differentiating (62) yields

$$\frac{\partial \Theta_{B2}}{\partial \xi} = e^{-\beta^2\tau}(-K_3\beta \sin\beta\xi + K_4\beta \cos\beta\xi). \tag{63}$$

Inserting this expression into the boundary condition (48) gives

$$K_4 = 0. \tag{64}$$

Applying the boundary condition (49) to (62) and (63) results in the transcendental equation

$$\beta \tan\beta = \nu. \tag{65}$$

An infinite number of values of β can satisfy the transcendental equation (65). Each value of β satisfying (65) is denoted by β_n, where n is a positive integer. Each β_n corresponds to a different value of K_3, which is labeled as $K_{3,n}$. Then the solution Θ_{B2} can be written as a sum of all possible solutions,

$$\Theta_{B2} = \sum_{n=1}^{\infty} K_{3,n} e^{-\beta_n^2 \tau} \cos \beta_n \xi. \tag{66}$$

The constant $K_{3,n}$ can now be determined by substituting (66) into the initial condition (57) with $\tau = 0$, giving

$$\Theta_0 + \frac{\lambda \xi^2}{2} - \lambda \left(\frac{1}{\nu} + \frac{1}{2} \right) = \sum_{n=1}^{\infty} K_{3,n} \cos \beta_n \xi. \tag{67}$$

To obtain $K_{3,n}$, multiply both sides of (67) by $\cos \beta_n \xi$ and integrate from 0 to 1. The resulting expression of $K_{3,n}$ is

$$K_{3,n} = \frac{\frac{\lambda \sin \beta_n}{2\beta_n} + \frac{\lambda \cos \beta_n}{\beta_n^2} - \frac{\lambda \sin \beta_n}{\beta_n^3} - \frac{\lambda \sin \beta_n}{\beta_n} \left(\frac{1}{\nu} + \frac{1}{2} \right) + \frac{\Theta_0 \sin \beta_n}{\beta_n}}{\frac{1}{2} + \frac{\sin \beta_n \cos \beta_n}{2\beta_n}}. \tag{68}$$

Thus, the complete solution to Problem B2 is

$$\Theta_{B2} = \sum_{n=1}^{\infty} \left(\frac{\frac{\lambda \sin \beta_n}{2\beta_n} + \frac{\lambda \cos \beta_n}{\beta_n^2} - \frac{\lambda \sin \beta_n}{\beta_n^3} - \frac{\lambda \sin \beta_n}{\beta_n} \left(\frac{1}{\nu} + \frac{1}{2} \right) + \frac{\Theta_0 \sin \beta_n}{\beta_n}}{\frac{1}{2} + \frac{\sin \beta_n \cos \beta_n}{2\beta_n}} \right) \times e^{-\beta_n^2 \tau} \cos \beta_n \xi. \tag{69}$$

3.1.3. Solution to Problem C

Problem C is the only problem that collects the information of the time-dependent boundary condition ($\sigma\tau$). A technique for solving this specific type of problems is *Duhamel's Theorem* (Lubecki, 2014). The solution to a similar problem by using Duhamel's Theorem is given in Carslaw and Jaeger (1959), and, with a few modifications, the exact solution to Problem C can be obtained as

$$\Theta_C = \sigma\tau + \sigma \left(\frac{\xi^2}{2} - \frac{1}{2} - \frac{1}{\nu} \right) + 2\nu\sigma \sum_{n=1}^{\infty} \frac{e^{-\beta_n^2 \tau} \cos \beta_n \xi}{\beta_n^2 \cos \beta_n \left(\nu^2 + \nu + \beta_n^2 \right)}, \tag{70}$$

where β_n satisfies the transcendental equation (65).

3.1.4. Exact solution to the original problem, Problem A

Summing the exact solutions to all subproblems gives the solution to the original problem,

$$\Theta = \Theta_A = \Theta_{B1} + \Theta_{B2} + \Theta_C, \tag{71}$$

where Θ_{B1}, Θ_{B2}, and Θ_C are given by (56), (69), and (70), respectively.

Eq. (71) is the exact solution for HFD. The exact solution for CFD is the same, by setting $\lambda = 0$. The exact solution for MFD is simpler as its temperature profile does not vary spatially due to the spatial symmetry of the problem. The model describing MFD is

$$\frac{\partial \Theta}{\partial \tau} = \lambda, \qquad 0 < \tau < \tau_m, \tag{72}$$

$$\Theta = \Theta_0, \qquad \tau = 0, \tag{73}$$

which can be integrated to yield the exact solution

$$\Theta = \Theta_0 + \lambda\tau. \tag{74}$$

3.2. Approximate solution for the heating stage

The analytical solution derived in the previous section is exact, that is, without error or approximation. The obtained exact solution for CFD and HFD contains infinite series with coefficients required to satisfy the transcendental equation, and thus cannot be written in closed form. In addition, the derivation procedure contains numerous steps and is relatively complicated, making it difficult to be adapted when there are some changes in the model, e.g., variation in the boundary condition. This section alternatively derives an approximate analytical solution to the freeze-drying model for CFD and HFD. The obtained solution is a closed-form expression and has a simpler derivation.

Firstly, assume that the approximate solution can be expressed by

$$\Theta = a_1(\tau) + a_2(\tau)\xi + a_3(\tau)\xi^2, \tag{75}$$

where a_1, a_2, and a_3 are the unknown functions of time τ to be determined. This expression is selected to be simplest while being able to satisfy the boundary conditions. Also, for a typical heat equation in the rectangular coordinate system, a second-degree polynomial has been observed to provide a good approximation (Goodman, 1964; Taler and Duda, 2006). Differentiating (75) results in

$$\frac{\partial \Theta}{\partial \xi} = a_2(\tau) + 2a_3(\tau)\xi, \tag{76}$$

$$\frac{\partial^2 \Theta}{\partial \xi^2} = 2a_3(\tau). \tag{77}$$

Substituting (76) in (23) gives

$$a_2 = 0. \tag{78}$$

Substituting (75) and (76) into (22), with some rearrangement, yields

$$a_1 + a_3 \left(1 + \frac{2}{\nu} \right) = \sigma\tau. \tag{79}$$

The boundary conditions are now satisfied, with a_1 and a_3 yet to be determined. At this stage, we employ the *integral method*, a useful technique widely used in the analysis of fluid flow, mass transfer, and heat transfer for approximating the solutions to complicated problems (Mills, 1995; Deen, 1998; Bird et al., 2002). In the integral method, the temperature is required to satisfy the heat-balance integral instead of the original governing equation (Goodman, 1964). The heat-balance integral can be obtained by integrating the governing equation (21),

$$\int_0^1 \frac{\partial \Theta}{\partial \tau} d\xi = \int_0^1 \frac{\partial^2 \Theta}{\partial \xi^2} d\xi + \int_0^1 \lambda d\xi. \tag{80}$$

Substitute (75), (77), and (79) into (80), apply the Leibniz integral rule (Petrovic, 2020) to the left-hand side, and integrate the equation to obtain

$$\left(-\frac{2}{3} - \frac{2}{\nu} \right) \frac{da_3}{d\tau} = 2a_3 + \lambda - \sigma. \tag{81}$$

The heat-balance integral converts the original PDE into the ODE (81). Solving the ODE is much simpler than solving the PDE, making this solution technique much simpler than that introduced in Section 3.1. Eq. (81) can be solved analytically with an appropriate initial condition. To determine the initial condition for a_3, i.e., a_3 at $\tau = 0$, we rely on the fact that the governing PDE is satisfied on the average, not exactly, as the equation is integrated over the spatial domain Goodman (1964). Hence, the initial condition of a_3 should be connected to the initial average temperature of the system. The average temperature is

$$\overline{\Theta} = \int_0^1 \Theta d\xi. \tag{82}$$

Substituting (75) into (82) yields

$$\overline{\Theta} = a_1 + \frac{a_3}{3}. \tag{83}$$

The initial average temperature can be obtained by integrating the initial condition (24), which is

$$\overline{\Theta} = \int_0^1 \Theta_0 d\xi = \Theta_0, \qquad \tau = 0. \tag{84}$$

Eqs. (79), (83), and (84) at $\tau = 0$ can be solved simultaneously for a_1 and a_3 to give the initial condition for a_3,

$$a_3 = -\frac{3\nu\Theta_0}{2\nu + 6}, \qquad \tau = 0. \tag{85}$$

Integrating (81) and applying the initial condition (85) give

$$a_3 = \left(\frac{\lambda}{2} - \frac{\sigma}{2} - \frac{3\nu\Theta_0}{2\nu+6}\right) e^{-\frac{3\nu}{\nu+3}\tau} - \frac{\lambda}{2} + \frac{\sigma}{2}, \tag{86}$$

$$a_1 = \sigma\tau - \left(1+\frac{2}{\nu}\right)\left(\left(\frac{\lambda}{2} - \frac{\sigma}{2} - \frac{3\nu\Theta_0}{2\nu+6}\right) e^{-\frac{3\nu}{\nu+3}\tau} - \frac{\lambda}{2} + \frac{\sigma}{2}\right). \tag{87}$$

Inserting these expressions and $a_2 = 0$ into (75) gives the approximate solution

$$\begin{aligned}\Theta = \sigma\tau - \left(1+\frac{2}{\nu}\right)\left(\left(\frac{\lambda}{2} - \frac{\sigma}{2} - \frac{3\nu\Theta_0}{2\nu+6}\right) e^{-\frac{3\nu}{\nu+3}\tau} - \frac{\lambda}{2} + \frac{\sigma}{2}\right) \\ + \xi^2\left(\left(\frac{\lambda}{2} - \frac{\sigma}{2} - \frac{3\nu\Theta_0}{2\nu+6}\right) e^{-\frac{3\nu}{\nu+3}\tau} - \frac{\lambda}{2} + \frac{\sigma}{2}\right).\end{aligned} \tag{88}$$

3.3. Exact solution for the sublimation stage

The above two sections derive analytical solutions to the freeze-drying model during the heating stage. For the sublimation stage, the governing equation (28) is much simpler, and the equation can be integrated directly, resulting in

$$\eta(\tau) = \frac{\kappa_1(\tau^2 - \tau_m^2)}{2} + \kappa_2(\tau - \tau_m), \qquad \tau_m < \tau \le \tau_{\max}. \tag{89}$$

When the shelf temperature reaches its maximum value $T_{b,\max}$ at $t_{\max}$ (or $\tau_{\max}$), the shelf temperature is constant, and thus the interface evolves linearly,

$$\eta(\tau) = \eta(\tau_{\max}) + (\kappa_1\tau_{\max} + \kappa_2)(\tau - \tau_{\max}), \qquad \tau > \tau_{\max}. \tag{90}$$

An approximate solution for the sublimation stage is not needed because the exact solution is a simple closed-form expression.

4. Numerical methods

The formulated model in Section 2 can be alternatively solved using numerical techniques. Introducing spatial discretization of the frozen region to produce N grid points ($i = 1$ to $i = N$), including the two boundaries, gives the distance between each grid point of

$$\Delta\xi = \frac{1}{N-1}. \tag{91}$$

This article develops two numerical solutions to the freeze-drying model, and these solutions are compared with the analytical solutions to cross-validate the models and solution procedures.

4.1. Finite difference-based method of lines

The first technique applies the finite difference method (FDM) for spatial discretization and the numerical method of lines (MOL) for time integration. The governing PDE is discretized spatially to produce a system of ODEs, and that system of ODEs can be integrated using available ODE solvers.

Prior to sublimation, spatial discretization of the governing PDE (21) using a central difference approximation leads to

$$\frac{d\hat{\Theta}_i}{d\tau} = \frac{\hat{\Theta}_{i+1} - 2\hat{\Theta}_i + \hat{\Theta}_{i-1}}{(\Delta\xi)^2} + \lambda, \qquad 2 \le i \le N-1, \tag{92}$$

where $\hat{\Theta}_i$ denotes the FDM solution at node i. The boundary condition (22) becomes

$$\frac{-\hat{\Theta}_{N+1} + \hat{\Theta}_{N-1}}{2\Delta\xi} = \nu(\hat{\Theta}_N - \sigma\tau). \tag{93}$$

The temperature at $i = N+1$ is not in the domain but can be eliminated by substituting this boundary condition into the governing PDE at node $i = N$, resulting in

$$\frac{d\hat{\Theta}_N}{d\tau} = \frac{-(2\Delta\xi\nu + 2)\hat{\Theta}_N + 2\hat{\Theta}_{N-1} + 2\Delta\xi\nu\sigma\tau}{(\Delta\xi)^2} + \lambda. \tag{94}$$

The discretized boundary condition (23) is

$$\frac{\hat{\Theta}_2 - \hat{\Theta}_0}{2\Delta\xi} = 0. \tag{95}$$

The temperature at $i = 0$ can be treated similarly as described for $i = N+1$, which gives

$$\frac{d\hat{\Theta}_1}{d\tau} = \frac{-2\hat{\Theta}_1 + 2\hat{\Theta}_2}{(\Delta\xi)^2} + \lambda. \tag{96}$$

For convenience, the system of Eqs. (92), (94), and (96) can be written in the matrix form

$$\frac{d\mathbf{x}_1}{d\tau} = \mathbf{A}_1\mathbf{x}_1 + \mathbf{b}_1(\tau), \tag{97}$$

where $\mathbf{x}_1 \in \mathbb{R}^{N\times 1}$ collects the FDM solution $\hat{\Theta}$, $\mathbf{A}_1 \in \mathbb{R}^{N\times N}$, and $\mathbf{b}_1 \in \mathbb{R}^{N\times 1}$. This system of equations can be integrated using `ode15s` in MATLAB.

During sublimation, (28) can be integrated analytically or numerically, but no spatial discretization is required. For consistency with the above model, the equation is integrated using `ode15s` in MATLAB.

4.2. Finite element-based method of lines

The technique presented in this section employs the finite element method (FEM) to discretize the spatial domain and the MOL for time integration. The major difference between the FDM and FEM is that the former is based on a strong formulation of the PDE, while the latter is derived from a weak formulation. The procedure to derive and apply the linear FEM for time-dependent PDEs with the MOL is well described in Chen et al. (1999) and Lin et al. (2013).

The FEM is capable of handling complex geometry better than the FDM as the elements can be developed in various shapes, which is more flexible than the finite difference grids (Strang, 2007). In addition, for a typical heat equation, the weak form used in the FEM involves only first derivatives, which is more convenient for treating functions/cases where second derivatives are not defined. Although these advantages are not relevant for the freeze-drying model considered here, the FEM provides a framework that is more readily extendable to handling more complicated geometry or radiation profiles.

First consider the model describing rising temperature before sublimation starts. The weak formulation of (21)–(23) is

$$\int_0^1 v\frac{\partial\Theta}{\partial\tau}d\xi = a(\Theta, v) + l(v), \qquad \forall v \in H^1(0,1), \tag{98}$$

where $H^1(0,1)$ is the Hilbert space over the domain of interest, $a(\Theta, v)$ is the bilinear form

$$a(\Theta, v) = -\int_0^1 \frac{\partial\Theta}{\partial\xi}\frac{\partial v}{\partial\xi}d\xi - \nu(v\Theta)_{\xi=1}, \tag{99}$$

and $l(v)$ is the linear form

$$l(v) = \int_0^1 v\lambda d\xi + \nu\sigma\tau v|_{\xi=1}. \tag{100}$$

In the linear FEM, the solution Θ is approximated as being piecewise linear. Here $\tilde{\Theta}$ denotes the FEM solution, which can be written as

$$\tilde{\Theta}(\xi,\tau) = \sum_{i=1}^{N}\tilde{\Theta}_i(\tau)\phi_i(\xi), \tag{101}$$

where the coefficient $\tilde{\Theta}_i(\tau)$ is the time-dependent dimensionless temperature at node i approximated using the linear FEM, and $\phi_i(\xi)$ is a triangular function serving as a nodal basis whose value is 1 only at node i and 0 at all other nodes $j \ne i$. Similarly, v can be approximated as

$$v(\xi,\tau) = \sum_{j=1}^{N} v_j(\tau)\phi_j(\xi). \tag{102}$$

Table 1
Default parameters in the simulations.

Parameter	Value	Unit	Reference
ρ	917	kg/m^3	Velardi and Barresi (2008)
ρ_a	63	kg/m^3	Velardi and Barresi (2008)
k	2.30	W/m K	Velardi and Barresi (2008)
C_P	1967.8	J/kg K	Velardi and Barresi (2008)
ΔH_{sub}	2.84 $\times$ 10^6	J/kg	Velardi and Barresi (2008)
H_w	242,345	W/m^3	Park et al. (2021)
p_{bw}	0.04	–	Park et al. (2021)
p_{ice}	0.96	–	Assumed to be 1 – p_{bw}
p_w	0.92	–	Park et al. (2021)
h	65	W/m^2 K	Hottot et al. (2006)
L	0.042	m	Park et al. (2021)
T_0	236.85	K	Gitter et al. (2019)
T_{b0}	236.85	K	Gitter et al. (2019)
T_m	256.15	K	Gitter et al. (2019)
$T_{b,\max}$	281.85	K	Park et al. (2021)
r	1	K/min	Park et al. (2021)
N	20	–	–
n	50	–	–

Substitute (101) and (102) into (98) and rearrange into the matrix form

$$\mathbf{M}\frac{d\mathbf{x}_2}{d\tau} = \mathbf{A}_2\mathbf{x}_2 + \mathbf{b}_2(\tau), \tag{103}$$

where $\mathbf{M} \in \mathbb{R}^{N\times N}$ is the mass matrix associated with time derivatives, $\mathbf{x}_2 \in \mathbb{R}^{N\times 1}$ collects the finite element solution $\tilde{\Theta}$, $\mathbf{A}_2 \in \mathbb{R}^{N\times N}$ is the matrix associated with the bilinear form (99), and $\mathbf{b}_2 \in \mathbb{R}^{N\times 1}$ is the vector associated with the linear form (100). The entries $M_{i,j}$ of $\mathbf{M}$, $(A_2)_{i,j}$ of $\mathbf{A}_2$, and $(b_2)_i$ of $\mathbf{b}_2$ are

$$M_{i,j} = \int_0^1 \phi_i\phi_j d\xi, \tag{104}$$

$$(A_2)_{i,j} = a(\phi_i, \phi_j), \tag{105}$$

$$(b_2)_i = l(\phi_i). \tag{106}$$

The system of ODEs (103) can also be integrated using `ode15s` in MATLAB.

For $\tau \geq \tau_m$, the model can be treated with the same approach described and used for the FDM.

5. Results and discussion

This section presents and discusses results obtained from simulating the exact, approximate analytical, FDM, and FEM solutions. Table 1 tabulates the default parameters used in this work.

5.1. Analysis of the exact solution

We firstly analyze the exact solution to the freeze-drying model. The exact solution is theoretically the most accurate solution, which is ideal for model-based designs that require extremely high accuracy. During the heating stage, the exact solution is given by (71) for CFD and HFD, and (74) for MFD. For the sublimation stage, the exact solution is expressed by (89) and (90).

Figs. 2–4 reveal the exact solutions for the temperature profile and sublimating interface position of the frozen material for CFD, MFD, and HFD, respectively. The temperature profile for CFD is similar to a parabolic curve (Fig. 2), which is a key assumption used to derive the approximate solution in Section 3.2. The temperature is highest at the bottom ($x = 0.042$ m) and becomes flat at the top ($x = 0$ m). The heating stage stops when the top surface temperature reaches the sublimation point of 256.15 K. The heating time is about 0.73 h before sublimation occurs, and the drying time is 17 h. The temperature for MFD increases linearly from the initial temperature of 236.85 K to the sublimation point of 256.15 K (Fig. 3). The temperature does not vary spatially as the microwave irradiation heats the frozen material uniformly. The heating and drying times are about 1.00 h and 3.90 h, respectively. In comparison with CFD, the heating time is higher, but the overall drying time can be shortened by about 77%. The temperature for HFD appears to be a combination of the MFD and CFD profiles (Fig. 4). The heating and drying times are about 0.57 h and 3.04 h, respectively. The total drying time is reduced by 82% compared with CFD and 22% compared with MFD. The reduction in the drying time is consistent with values reported in the literature (Gitter et al., 2018; Bhambhani et al., 2021; Park et al., 2021).

The exact solution for CFD and HFD derived in Section 3.1 contains two infinite series, (69) and (70). Including more terms (n) in the infinite series improves the accuracy of the solution but increases the computational cost, with each term requiring the solution of the transcendental Eq. (65). In fact, only a few terms in the infinite series are required to obtain a highly accurate solution. By using HFD as an example, Fig. 5 shows that the first term ($n = 1$) is much larger than any other terms in the series. For $\tau = 0$, the contribution from the second term is about 1%–2% of the first term, with much smaller contribution from the rest. For $\tau \geq 0.2$, only the first term in the series has a significant contribution, whereas other terms vanish to 0 (within machine precision) quickly, and this decrease becomes more abrupt as time progresses (higher values of τ). This behavior is consistent with the result discussed by Mills (1995). Fig. 6 provides more insight into the errors between the solution with $n = 1$ (sometimes known as one-term solutions) and solution with $n = 50$. The maximum error of around 0.2 K (less than 0.1% of the actual initial temperature, 236.85 K) occurs at $\tau = 0$, and this error rapidly decreases with time, which is consistent with the contribution of each term shown in Fig. 5. From this analysis, only the first term in the infinite series is needed to obtain accurate solutions for this system. The only exception could be when extremely high accuracy is required for small values of τ, in which case adding the second or third term into the series could be an option. This analysis also justifies that $n = 50$ used in Figs. 2 and 4 is sufficient to produce results that are accurate within machine precision. To avoid confusion, the *exact solution* refers to the analytical solution with $n = 50$ and the *one-term solution* refers to the analytical solution with $n = 1$ in the rest of this article.

5.2. Analysis of the approximate solution

The approximate solution derived using the integral method in Section 3.2 for CFD and HFD during the heating stage is given by (88). Its temperature profiles in Fig. 7 are visually nearly identical to the exact solution (Figs. 2 and 4). The difference between the approximate and exact solutions is about 0.2–0.3 K (Fig. 8), which is only 0.1% of the actual temperature. For CFD, the approximate and exact heating times are 0.7366 and 0.7316 h, respectively. For HFD, the approximate and exact heating times are 0.5729 h and 0.5689 h, respectively. The error between the approximate and exact heating times is less than 1%.

As shown and described above, the approximate solution derived by the integral method provides a highly accurate prediction of the temperature profiles and heating times for both CFD and HFD. Since the approximate solution is much simpler and can be written in closed form, it is useful for tasks where a large number of parameters need to be varied, including parametric studies, optimization, and optimal control of the freeze-drying system, which is demonstrated in Section 5.4.

5.3. Comparison between the analytical and numerical solutions

The freeze-drying model can be solved numerically using the FDM and FEM as explained in Section 4. Here the numerical solutions are compared with the analytical solutions to cross-validate the obtained solutions.

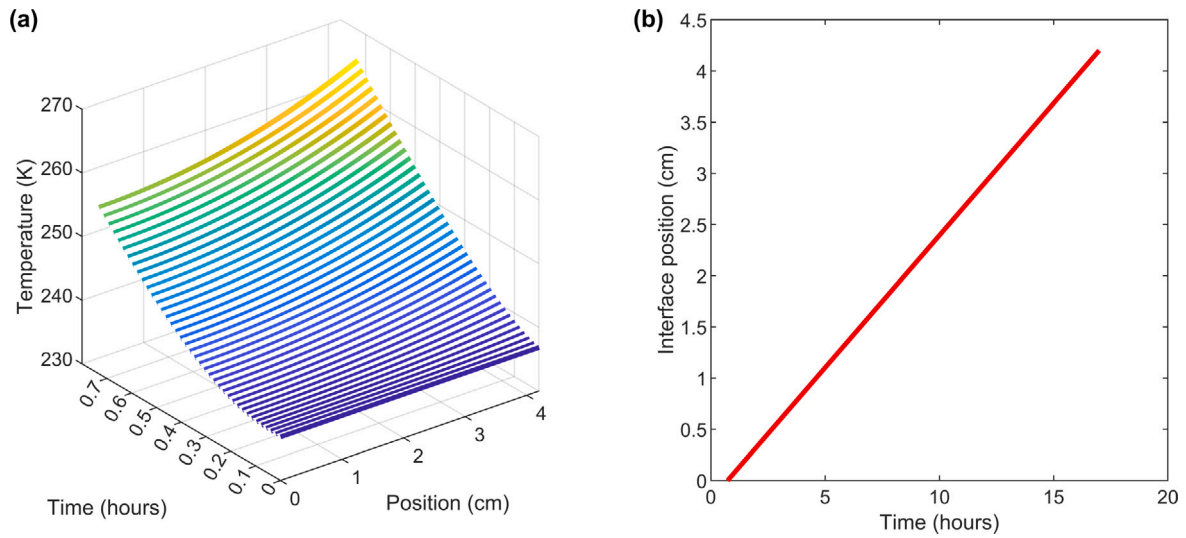

Fig. 2. Exact solutions for CFD with $n = 50$ for the (a) spatiotemporal evolution of the frozen material temperature during the heating stage and (b) time evolution of the interface position during the sublimation stage.

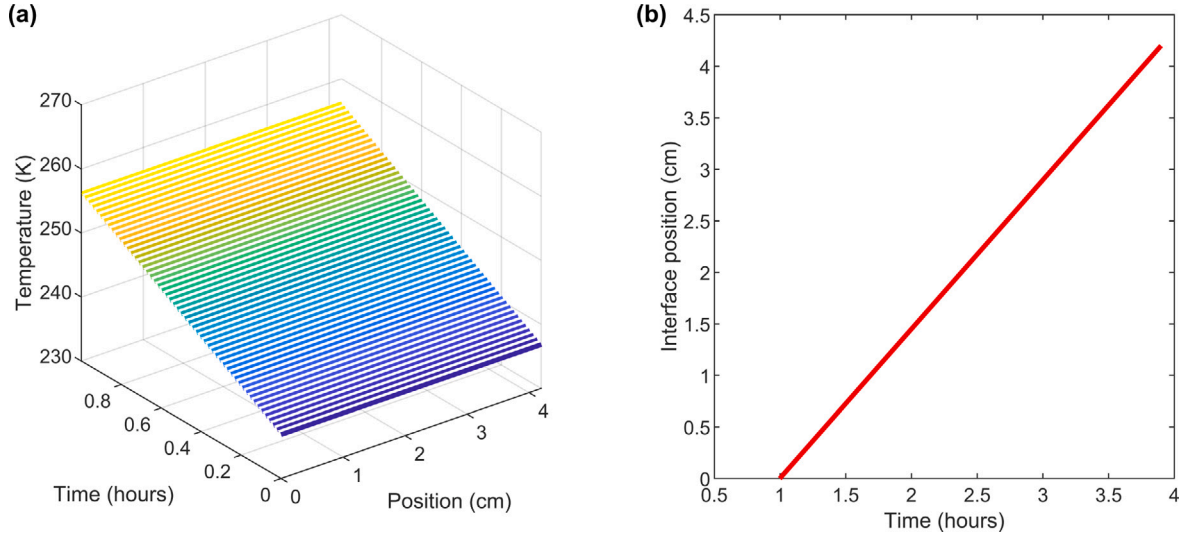

Fig. 3. Exact solutions for MFD for the (a) spatiotemporal evolution of the frozen material temperature during the heating stage and (b) time evolution of the interface position during the sublimation stage.

The temperature differences between the analytical and numerical solutions during the heating stage are analyzed first. In this error analysis, the results for HFD are presented only because HFD is the most generic and complicated scenario; CFD is a special case of HFD in which $\lambda = 0$, and MFD has a very simple analytical solution in which the temperature increases linearly with time. The numerical solutions (both FDM and FEM) are different from the exact solution by about 10^{-3} K (Fig. 9a), indicating that the FDM and FEM solutions are highly accurate. The error between the approximate and numerical solutions ranges between 0.1–0.25 K (Fig. 9b), which is similar to the error between the exact and approximate solutions (Fig. 8).

Table 2 compares the heating and drying times predicted by all the solutions. For CFD and HFD, the error between the numerical and exact solutions is about 10^{-4} h, which is too small to be detected in the real system. The accuracy of the approximate solution is as discussed in Section 5.2. For MFD, the error between the numerical and exact solutions is within machine precision.

Every solution method presented in this article is highly accurate for all freeze-drying modes (CFD, MFD, and HFD). The exact solution contains infinite terms and requires solving a transcendental equation to obtain the coefficient for each term in the infinite series. The advantage of the numerical solutions is that it can be applied to more complicated models in which the analytical solutions are not readily available. Finally, the approximate solution may not be as accurate as the exact or numerical solution, but is much cheaper to implement while providing high accuracy (error < 1%). Consequently, the approximate solution can be useful in tasks in which the solution is embedded in a more complicated calculation, e.g., optimization and model-based control, as demonstrated in the next section.

Table 2
Heating and drying times predicted by the exact, approximate, FDM, and FEM solutions.

Solution technique	Heating time (hours)			Total dying time (hours)		
	CFD	MFD	HFD	CFD	MFD	HFD
Exact solution	0.7316	0.9980	0.5689	16.9930	3.8988	3.0364
Approximate solution	0.7366	–	0.5729	16.9978	–	3.0402
FDM solution	0.7317	0.9980	0.5690	16.9930	3.8988	3.0364
FEM solution	0.7316	0.9980	0.5690	16.9931	3.8988	3.0365

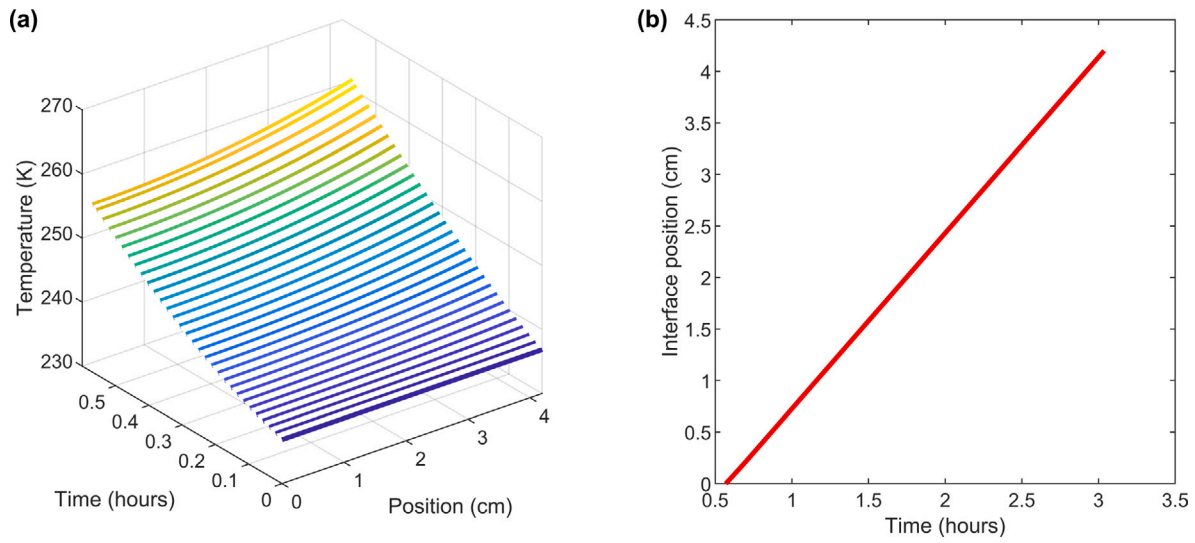

Fig. 4. Exact solutions for HFD with $n = 50$ for the (a) spatiotemporal evolution of the frozen material temperature during the heating stage and (b) time evolution of the interface position during the sublimation stage.

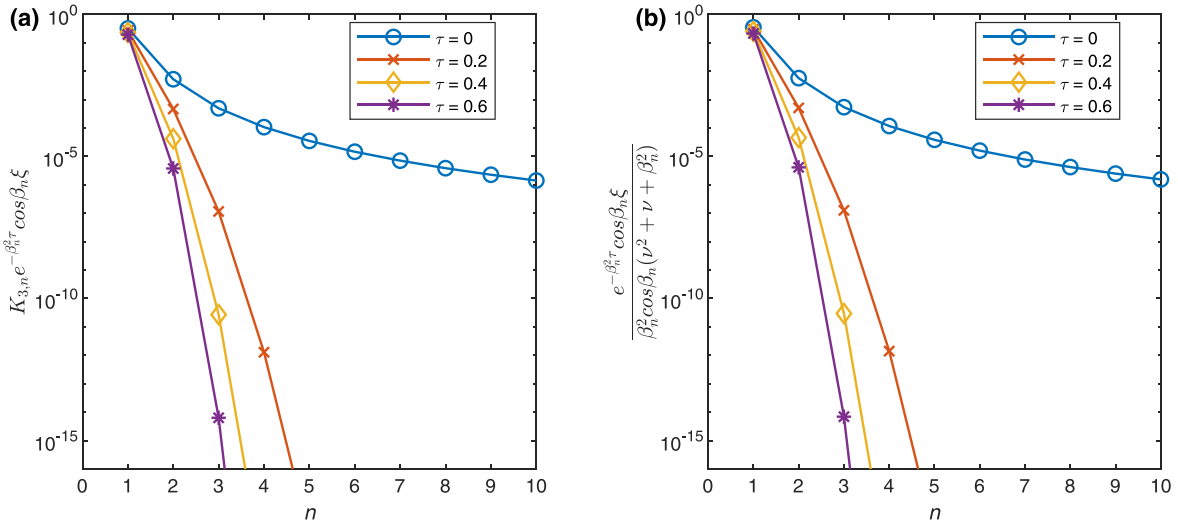

Fig. 5. Contribution of the first ten terms in the infinite series defined in (a) Problem B2 and (b) Problem C for HFD. The value of each term is evaluated at the bottom surface during the heating stage.

5.4. Case studies

We have shown in the previous sections that the approximate analytical solution can provide highly accurate prediction of spatiotemporal evolution of temperature during the primary drying stage. In addition, the simple closed-form expression does not require solving any transcendental equation or numerical treatment. As such, the approximate solution is highly suitable for incorporation into optimization-based design and control problems. This section presents some examples of using the approximate solution for solving such problems.

5.4.1. Parameter estimation

A key parameter in freeze-drying modeling is the heat transfer coefficient (h_b; ν in dimensionless form) as it governs the heat transfer characteristics in the system (Fissore et al., 2018; Wegiel et al., 2018). Various techniques for fitting the heat transfer coefficient to experimental data have been explored, with one of the most commonly used techniques based on measurement of the weight loss of ice and bottom temperature as a function of time during sublimation (Pikal et al., 1984; Fissore et al., 2015; Wegiel et al., 2018).

An alternative fast and simple way to estimate the heat transfer coefficient uses the approximate solution (88). Unlike past techniques, the only information needed is accurate temperature measurement during the heating process ($\Theta(\tau)$); i.e., no phase change data are required. If there is only one data point, the heat transfer coefficient can be estimated simply by solving

$$\begin{aligned}\Theta_{\text{exp}} = \sigma\tau_{\text{exp}} - \left(1+\frac{2}{\nu_{\text{est}}}\right)\left(\left(\frac{\lambda}{2}-\frac{\sigma}{2}-\frac{3\nu_{\text{est}}\Theta_0}{2\nu_{\text{est}}+6}\right)\right.\\ \left.\times e^{\left(-\frac{3\nu_{\text{est}}}{\nu_{\text{est}}+3}\right)\tau_{\text{exp}}}-\frac{\lambda}{2}+\frac{\sigma}{2}\right)\\ +\xi^2\left(\left(\frac{\lambda}{2}-\frac{\sigma}{2}-\frac{3\nu_{\text{est}}\Theta_0}{2\nu_{\text{est}}+6}\right)e^{\left(-\frac{3\nu_{\text{est}}}{\nu_{\text{est}}+3}\right)\tau_{\text{exp}}}-\frac{\lambda}{2}+\frac{\sigma}{2}\right),\end{aligned} \tag{107}$$

where Θ_{exp} is the measured temperature, τ_{exp} is the corresponding time, ν_{est} is the estimated heat transfer coefficient, and the other parameters are the properties of that experimental system. Eq. (107) can be solved easily by plotting the right-hand side as a function of ν_{est} to see where its value is equal Θ_{exp} or by using a nonlinear solver. It is common to have more than one temperature data point from the experiment, which can be used to give a more accurate value of ν_{est} by solving the

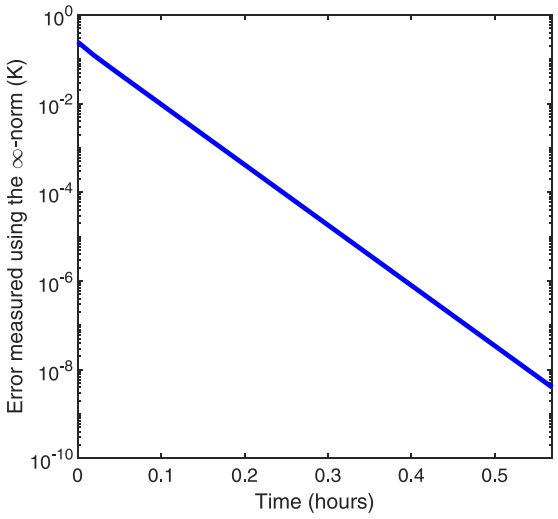

Fig. 6. Time evolution of the temperature difference between the solution with $n = 1$ and solution with $n = 50$ for HFD during the heating stage. Errors are measured using the ∞-norm.

optimization problem

$$v_{\text{est}} = \arg\min_{v} \sum_{l=1}^{n_d} (\Theta_{\text{exp},l} - \Theta_{\text{approx},l}(v))^2, \tag{108}$$

where n_d is the total number of data points available, $\Theta_{\text{exp},l}$ denotes the individual measured temperature (one data point), and $\Theta_{\text{approx},l}$ is the approximate temperature calculated by (88) at the time corresponding to $\Theta_{\text{exp},l}$. Eq. (108) minimizes the 2-norm of the error between the actual and approximate temperature profiles, which can be solved by reading the minimum from a plot of the right-hand side of (108) or by using a nonlinear optimization solver.

To demonstrate, the above technique was employed to estimate the heat transfer coefficient using the experimental data in Velardi and Barresi (2008). In their experiment, the shelf temperature was increased with the rate of 0.25 K/min from 228.5 K to 268.15 K, the measured temperature of the frozen material considering the potential bias in measurement was around 235.11–238.20 K at 0.77 h after the heating started, the initial thickness was 7.15×10^{-3} m, and no microwave term ($\lambda = 0$) was considered. Other parameters are as tabulated in Table 1. By substituting this information into (107) and solving the equation using MATLAB's `fsolve`, the estimated heat transfer coefficient is about 10.44–35.82 W/m^2 K, which agrees well with the mean value of 20.25 W/m^2 K used in Velardi and Barresi (2008) and is consistent with the typical range of a heat transfer coefficient in freeze drying (Hottot et al., 2005).

5.4.2. Optimal control

Primary drying is usually the longest and most expensive step in freeze drying, and hence this stage is the main focus of process control and optimization (Velardi and Barresi, 2008; Pisano et al., 2010). Productivity is maximized by minimizing the drying time required during primary drying (Fissore et al., 2018), which can be achieved by maximizing the shelf temperature to shorten the heating stage and maximize the rate of sublimation. Practical constraints are to ensure that (1) the temperature of the product is not so high that the lyophilized cake collapses, and (2) the rate of vapor production does not exceed the condenser capacity to avoid vapor accumulation and choked flow, which can lead to overpressure in the chamber (Fissore et al., 2018; Bano et al., 2020). Model-based dynamic optimization (aka optimal control) has been formulated and numerical solved for primary drying in CFD (Bano et al., 2020) to manipulate the shelf temperature to minimize the drying time while maintaining the product temperature and rate of vapor production below their limits.

Table 3
Parameters used in the optimal control problem.

Parameter	Value	Unit
$r_{\max}$	1	K/min
$H_{w,\min}$	180,000	W/m^3
$H_{w,\max}$	320,000	W/m^3
$(ds/dt)_{\max}$	0.0273	cm/min

This section illustrates the use of the simplified model and corresponding analytical solutions for fast and efficient optimal control of primary drying. The problem formulation is similar to that of Bano et al. (2020) with three main differences: (1) HFD is considered rather than CFD, (2) the microwave term (H_w) is included as another manipulated variable (in addition to the shelf temperature, T_b), and (3) our approximate analytical solution is used rather than the numerical solution. In our model, the evolution of the sublimating interface ds/dt is the speed of sublimation, and thus can be used to reflect the rate of vapor production. The optimal control problem can be formulated as

$$\min_{T_b(t), H_w(t)} t_f \tag{109}$$

subject to

Eqs. (2)–(12),

$$0 \le r \le r_{\max}, \tag{110}$$

$$T_b \le T_{b,\max}, \tag{111}$$

$$H_{w,\min} \le H_w \le H_{w,\max}, \tag{112}$$

$$\frac{ds}{dt} \le \left(\frac{ds}{dt}\right)_{\max}, \tag{113}$$

where t_f is the final time or total drying time, $r_{\max}$ is the highest temperature ramp-up rate, $T_{b,\max}$ is the maximum shelf temperature given in Table 1, $H_{w,\min}$ and $H_{w,\max}$ are the minimum and maximum microwave power, and $(ds/dt)_{\max}$ is the maximum sublimation rate. The first set of constraints (2)–(12) ensures that the governing equation, initial condition, and boundary conditions are all satisfied throughout the process; (2)–(7) describe the heating stage; (9)–(12) govern the sublimation stage; and (8) is the switching criterion. The constraint (110) defines the upper limit of the shelf temperature ramp-up rate. Eq. (111) ensures that the shelf temperature does not exceed the maximum value. Eq. (112) specifies the bounds on the microwave power. Lastly, the constraint (113) limits the sublimation rate to ensure that the rate of vapor production does not exceed the condenser capacity. The parameters used specifically for the optimal control problem are in Table 3.

The usual approach for solving optimal control problems is to discretize the PDE and ODE constraints, parameterize the time-varying manipulated variables, and solve the resulting optimization problem numerically (e.g., by using `fmincon` in MATLAB). During the heating stage in our problem, we can alternatively replace (2)–(7) with the approximate analytical solution (88), which is an algebraic equation. This substitution transforms the PDE and ODE constraints into an algebraic equation, reduces the number of equations, and eliminates the use of any numerical discretization. For the sublimation stage, the original Eqs. (9)–(12) are maintained as this problem focuses on controlling the rate of vapor production ds/dt rather than the exact position of the interface s, and so the analytical expression of s is not needed.

To minimize the drying time, the shelf temperature should be increased as fast as possible, and the microwave power should be maximized, forcing the constraints (110) and (112) to be active at the beginning. If the shelf temperature reaches its maximum value $T_{b,\max}$, the constraint (111) becomes active, and thus r becomes zero as the shelf temperature cannot be increased further. When the sublimation

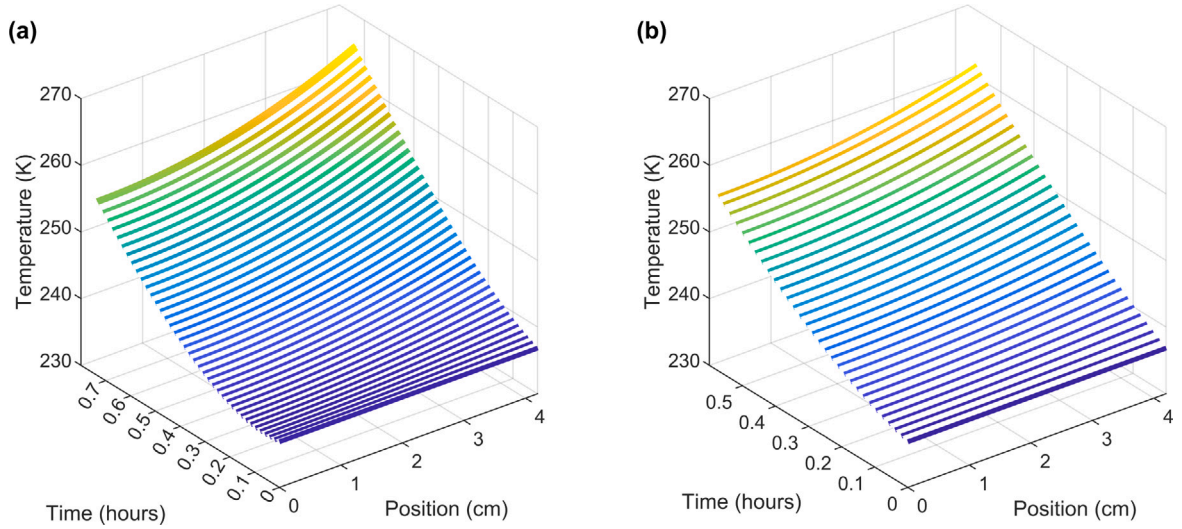

Fig. 7. Approximate solutions for (a) CFD and (b) HFD for the spatiotemporal evolution of the frozen material temperature during the heating stage.

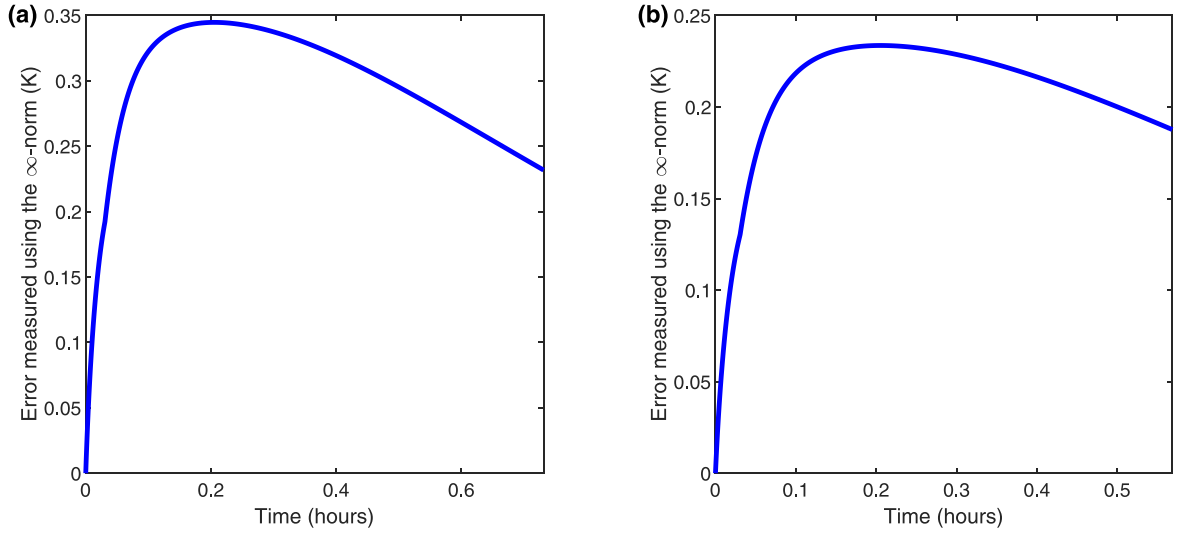

Fig. 8. Time evolution of the temperature difference between the approximate and exact solutions for (a) CFD and (b) HFD during the heating stage. Errors are measured using the ∞-norm.

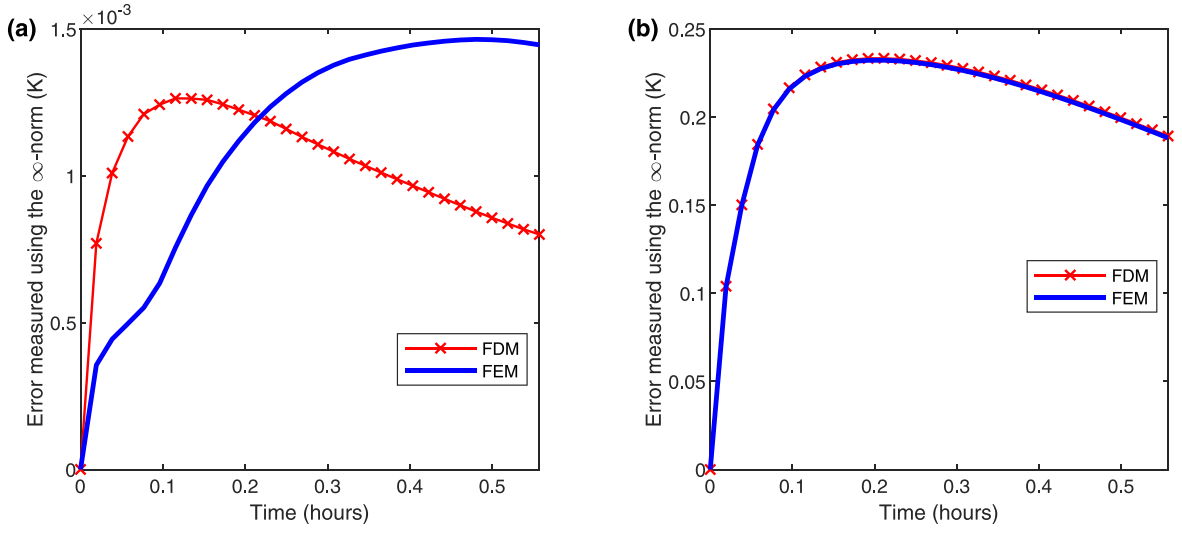

Fig. 9. Time evolution of the temperature difference between (a) the numerical and exact solutions, and (b) the numerical and approximate solutions for HFD during the heating stage. Errors are measured using the ∞-norm.

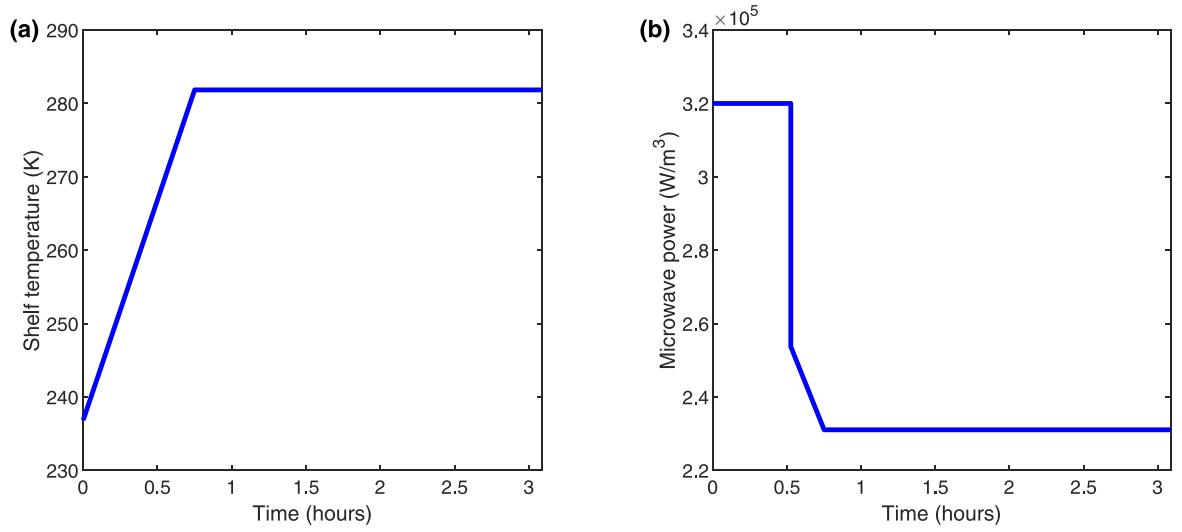

Fig. 10. Time evolution of the optimal (a) shelf temperature and (b) microwave power which minimizes the drying time during the primary drying stage in HFD.

Table 4
Parameters used in the parameter space analysis.

Parameter	Range	Increment	Unit
H_w	180,000 to 320,000	20,000	W/m^3
r	0.25 to 1	0.25	K/min
L	3 to 6	0.5	cm

rate ds/dt reaches the upper bound, the constraint (113) becomes active. The optimal temperature and microwave power profiles can be determined by identifying the active constraints and then solving those algebraic equations using a nonlinear algebraic equation solver, e.g., `fsolve` in MATLAB. This simulation-based technique eliminates the need for an optimization solver, resulting in a more computationally efficient solution to the optimal control problem (Berliner et al., 2022).

The optimal values of the shelf temperature and microwave power are shown in Fig. 10. The optimal shelf temperature increases linearly at the maximum ramp-up rate of 1 K/min from the initial temperature of 236.85 K to the maximum value of 281.85 K, and then the temperature is kept at its upper bound until the end of the drying process (Fig. 10a). The optimal microwave power is constant at its maximum value of 320,000 W/m^3 during the heating stage before decreasing abruptly to around 250,000 W/m^3 when sublimation starts to prevent excessive vapor production. After that, the microwave power reduces linearly to compensate for an increase in the shelf temperature, and eventually becomes stable at about 230,000 W/m^3 when the shelf temperature is constant (Fig. 10b). With the optimal shelf temperature and microwave power, the minimum drying time is about 3.1 h, with all process constraints satisfied throughout the primary drying.

5.4.3. Parameter space analysis

The accuracy of each solution is reported in Sections 5.1–5.3. This section investigates the computational performance of each solution technique for parameter space analysis, which requires a significant amount of simulation runs. The effects of the shelf temperature ramp-up rate (r), microwave power (H_w), and sample depth/height (L) on the drying time are explored. Table 4 tabulates the ranges and values of the parameters considered in this study, which results in a total of 224 simulation cases. Other parameters are set to the default values in Table 1.

The simulations were performed in MATLAB R2022a on a computer equipped with an AMD Ryzen™ 9 5900HS CPU and 32 GB RAM on Windows 10 64 bits. The wall-clock times measured using the `tic` and `toc` functions and the maximum errors in drying time prediction

Table 5
Wall-clock times and maximum errors in drying time prediction of the exact, one-term, FDM, FEM, and approximate solutions for the parameter space analysis.

Solution technique	Wall-clock time (s)	Maximum error (%)
Exact solution	200.23	–
One-term solution	6.00	2.77×10^{-5}
FDM solution	4.56	2.13×10^{-4}
FEM solution	4.46	2.30×10^{-3}
Approximate solution	1.00	0.43

(compared to the exact solution) are reported in Table 5. Simulating the exact solution ($n = 50$) is extremely slow because it requires solving the transcendental equation (65), which is computationally expensive; for $n = 50$, the number of transcendental equations to be solved is 50. Even for the one-term solution (one transcendental equation), the simulation time is higher than for the numerical and approximate solutions. The fastest solution technique is the approximate solution, which takes 25% as much time as the numerical solutions, 17% as much time as the one-term solution, and 0.5% as much time as the exact solution. In terms of deviation from the exact solution, the one-term solution is most accurate, followed by the FDM, FEM, and approximate solutions, respectively. The maximum error of the approximate solution among all 224 cases is less than 0.5%, which is highly accurate and sufficient for applications; e.g., for the drying time of 2 h, the error is only 1 min.

The maximum drying time among all 224 cases is about 5 h, which occurs for the lowest microwave power, lowest shelf temperature ramp-up rate, and largest sample size as expected (Fig. 11a). On the other hand, the minimum drying time is about 2.4 h, which occurs for the highest microwave power, highest shelf temperature ramp-up rate, and smallest sample size (Fig. 11d). Increasing the microwave power from 180,000 to 320,000 W/m^3 while the other two variables are fixed reduces the drying time by about 1.5–2 h. Increasing the shelf temperature ramp-up rate can decrease the drying time by about 1 h, which mostly influences the heating stage. The drying time is affected slightly (<30 min) when varying the sample size from 3 to 6 cm. Within this parameter space, the microwave power is the most significant design variable, agreeing with the result reported in Park et al. (2021).

All the results and case studies in this work have the maximum error of the approximate solution less than 1%. This error is relatively small compared to model uncertainties and measurement errors (Pikal et al., 2005; Velardi and Barresi, 2008); hence, the approximate solution can be confidently used to guide the design of a freeze-drying system

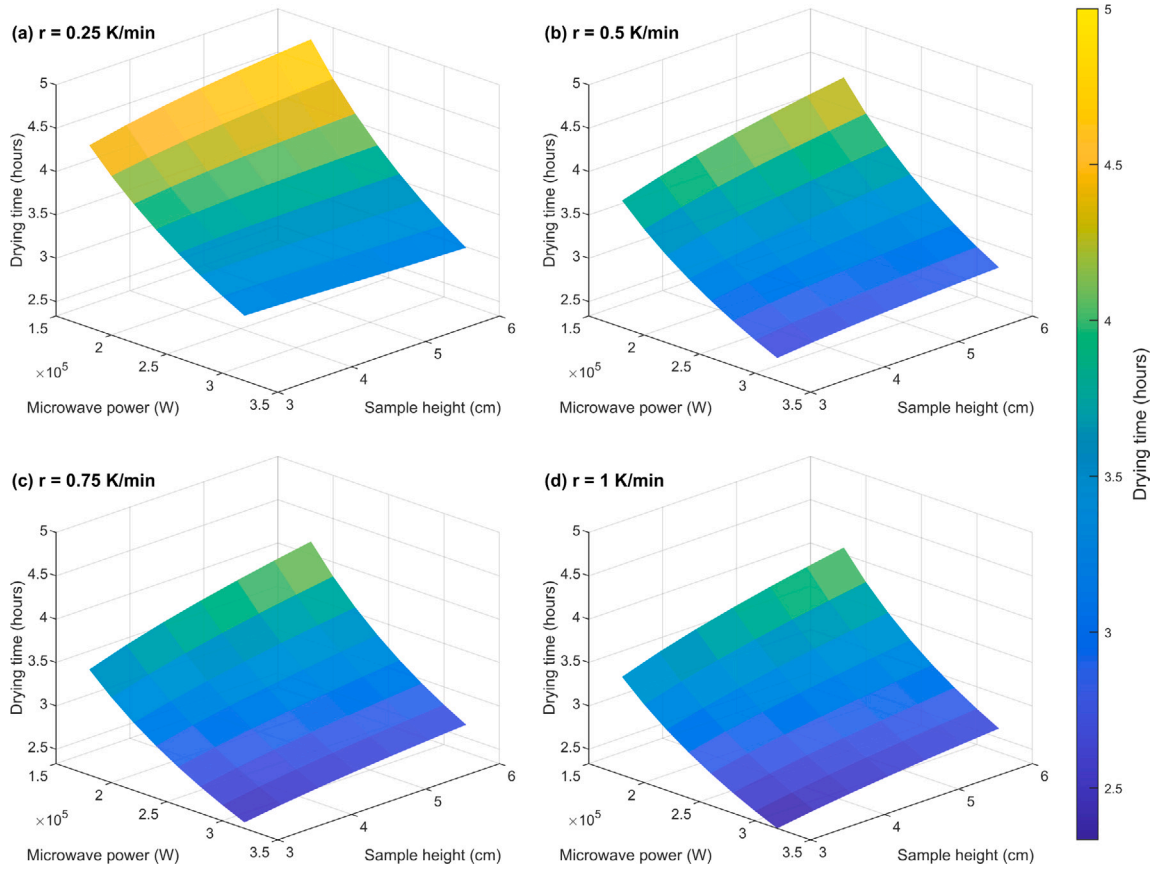

Fig. 11. Drying times required for primary drying in HFD under different conditions considered in the parameter space analysis. The microwave power H_w ranges from 180,000 to 320,000 W/m^3 with an increment of 20,000 W/m^3. The shelf temperature ramp-up rate r ranges from 0.25 to 1 K/min with an increment of 0.25 K/min. The sample height L ranges from 3 to 6 cm with an increment of 0.5 cm.

within the given parameter space and design conditions. In actual implementation, error in the approximate solution can be reduced by employing parameter estimation using experimental data as discussed in Section 5.4.1. The uncertainty in the approximate solution is small enough that its presence would not significantly affect the performance of a model-based monitoring and control system (Fissore et al., 2018).

6. Conclusion

Exact and approximate analytical solutions are derived for a mechanistic model of microwave-assisted freeze drying, which can also be applied to conventional and hybrid freeze drying. The exact solution can be derived using the superposition principle, separation of variables, and Duhamel's theorem, which involves infinite series and solving a transcendental equation. Alternatively, the approximate solution obtained via the heat-balance integral can be written as a simple closed-form expression and does not entail any transcendental equation.

In terms of accuracy, the exact solution is most accurate, up to machine precision, and so can be used as a reference solution to validate any numerical/approximate results. The approximate solution produces the maximum error in drying time and temperature predictions of less than 1% in the given parameter space. Regarding computational performance, the approximate solution can be computed fastest among all the solution techniques, which is about 4-fold and 200-fold faster than the numerical and exact solutions, respectively. With its high accuracy and computational performance, the approximate solution offers an efficient tool for design and optimization of the lyophilizer, which is demonstrated for parameter estimation, optimal control, and parameter space analysis.

Future work could consider more complicated models which may simulate microwave irradiation more accurately and take into account additional parameters such as pressure and concentration, so that optimization and control of the process can be done with higher degrees of freedom. Mathematical modeling of secondary drying in microwave-assisted freeze drying is also important as it can be another mean of optimizing the whole freeze-drying process.

CRediT authorship contribution statement

Prakitr Srisuma: Formal analysis, Funding acquisition, Investigation, Methodology, Software, Validation, Visualization, Writing – original draft, Writing – review & editing. **George Barbastathis:** Project administration, Supervision, Writing – review & editing. **Richard D. Braatz:** Formal analysis, Conceptualization, Funding acquisition, Methodology, Project administration, Resources, Supervision, Validation, Visualization, Writing – original draft, Writing – review & editing.

Declaration of competing interest

The authors declare that they have no known competing financial interests or personal relationships that could have appeared to influence the work reported in this paper.

Data availability

The MATLAB code used for generating the analytical and numerical solutions in this work is available at https://github.com/PrakitrSrisuma/Microwave-Lyophilization.

Acknowledgments

This research was supported by the U.S. Food and Drug Administration under the FDABAA-22-00123 program and, in part, by a Fulbright Program grant sponsored by the Bureau of Educational and Cultural Affairs of the U.S. Department of State and administered by the Institute of International Education.

References

Bano, G., De-Luca, R., Tomba, E., Marcelli, A., Bezzo, F., Barolo, M., 2020. Primary drying optimization in pharmaceutical freeze-drying: A multivial stochastic modeling framework. Ind. Eng. Chem. Res. 59 (11), 5056–5071. http://dx.doi.org/10.1021/acs.iecr.9b06402.

Barresi, A.A., Pisano, R., Fissore, D., Rasetto, V., Velardi, S.A., Vallan, A., Parvis, M., Galan, M., 2009. Monitoring of the primary drying of a lyophilization process in vials. Chem. Eng. Process. 48 (1), 408–423. http://dx.doi.org/10.1016/j.cep.2008.05.004.

Berliner, M.D., Jiang, B., Cogswell, D.A., Bazant, M.Z., Braatz, R.D., 2022. Novel operating modes for the charging of lithium-ion batteries. J. Electrochem. Soc. 169 (10), 100546. http://dx.doi.org/10.1149/1945-7111/ac9a80.

Bhambhani, A., Stanbro, J., Roth, D., Sullivan, E., Jones, M., Evans, R., Blue, J., 2021. Evaluation of microwave vacuum drying as an alternative to freeze-drying of biologics and vaccines: The power of simple modeling to identify a mechanism for faster drying times achieved with microwave. AAPS PharmSciTech 22 (1), 52. http://dx.doi.org/10.1208/s12249-020-01912-9.

Bird, R.B., Lightfoot, E.N., Stewart, W.E., 2002. Transport Phenomena, second ed. John Wiley & Sons, New York.

Carslaw, H., Jaeger, J., 1959. Conduction of Heat in Solids, second ed. Oxford University Press, London.

Chen, X., Sadineni, V., Maity, M., Quan, Y., Enterline, M., Mantri, R.V., 2015. Finite element method (FEM) modeling of freeze-drying: Monitoring pharmaceutical product robustness during lyophilization. AAPS PharmSciTech 16, 1317–1326. http://dx.doi.org/10.1208/s12249-015-0318-9.

Chen, R., Yung, E.K.N., Wu, K., Wang, D., 1999. Method of lines based on finite element discrete technique to analyze eigenvalues of waveguides. Int. J. Infrared Millim. Waves 20 (6), 1143–1153. http://dx.doi.org/10.1023/A:1021780708001.

Deen, W., 1998. Analysis of Transport Phenomena. Oxford University Press, New York.

Fissore, D., Pisano, R., Barresi, A.A., 2015. Using mathematical modeling and prior knowledge for QbD in freeze-drying processes. In: Jameel, F., Hershenson, S., Khan, M.A., Martin-Moe, S. (Eds.), Quality by Design for Biopharmaceutical Drug Product Development. Springer, New York, pp. 565–593. http://dx.doi.org/10.1007/978-1-4939-2316-8_23.

Fissore, D., Pisano, R., Barresi, A.A., 2018. Process analytical technology for monitoring pharmaceuticals freeze-drying – A comprehensive review. Dry. Technol. 36 (15), 1839–1865. http://dx.doi.org/10.1080/07373937.2018.1440590.

Gitter, J.H., Geidobler, R., Presser, I., Winter, G., 2018. Significant drying time reduction using microwave-assisted freeze-drying for a monoclonal antibody. J. Pharm. Sci. 107 (10), 2538–2543. http://dx.doi.org/10.1016/j.xphs.2018.05.023.

Gitter, J.H., Geidobler, R., Presser, I., Winter, G., 2019. Microwave-assisted freeze-drying of monoclonal antibodies: Product quality aspects and storage stability. Pharmaceutics 11 (12), http://dx.doi.org/10.3390/pharmaceutics11120674.

Goodman, T.R., 1964. Application of integral methods to transient nonlinear heat transfer. In: Irvine, T.F., Hartnett, J.P. (Eds.), Advances in Heat Transfer, Vol. 1. Academic Press, New York, pp. 51–122.

Hammerling, M.J., Warfel, K.F., Jewett, M.C., 2021. Lyophilization of premixed COVID-19 diagnostic RT-qPCR reactions enables stable long-term storage at elevated temperature. Biotechnol. J. 16 (7), 2000572. http://dx.doi.org/10.1002/biot.202000572.

Hottot, A., Peczalski, R., Vessot, S., Andrieu, J., 2006. Freeze-drying of pharmaceutical proteins in vials: Modeling of freezing and sublimation steps. Dry. Technol. 24 (5), 561–570. http://dx.doi.org/10.1080/07373930600626388.

Hottot, A., Vessot, S., Andrieu, J., 2005. Determination of mass and heat transfer parameters during freeze-drying cycles of pharmaceutical products.. PDA J. Pharm. Sci. Technol. 59 (2), 138–153.

Klepzig, L.S., Juckers, A., Knerr, P., Harms, F., Strube, J., 2020. Digital twin for lyophilization by process modeling in manufacturing of biologics. Processes 8 (10), 1325. http://dx.doi.org/10.3390/pr8101325.

Lin, T., Lin, Y., Zhang, X., 2013. A method of lines based on immersed finite elements for parabolic moving interface problems. Adv. Appl. Math. Mech. 5 (4), 548–568. http://dx.doi.org/10.4208/aamm.13-13S11.

Litchfield, R., Liapis, A., 1979. An adsorption-sublimation model for a freeze dryer. Chem. Eng. Sci. 34 (9), 1085–1090. http://dx.doi.org/10.1016/0009-2509(79)85013-7.

Lubecki, S., 2014. Duhamel's theorem for time-dependent thermal boundary conditions. In: Hetnarski, R.B. (Ed.), Encyclopedia of Thermal Stresses. Springer Netherlands, Dordrecht, pp. 1033–1040. http://dx.doi.org/10.1007/978-94-007-2739-7_379.

Mascarenhas, W., Akay, H., Pikal, M., 1997. A computational model for finite element analysis of the freeze-drying process. Comput. Methods Appl. Mech. Engrg. 148 (1), 105–124. http://dx.doi.org/10.1016/S0045-7825(96)00078-3.

Mills, A., 1995. Heat and Mass Transfer. Routledge, New York, http://dx.doi.org/10.4324/9780203752173.

Park, J., Cho, J.H., Braatz, R.D., 2021. Mathematical modeling and analysis of microwave-assisted freeze-drying in biopharmaceutical applications. Comput. Chem. Eng. 153, 107412. http://dx.doi.org/10.1016/j.compchemeng.2021.107412.

Petrovic, J., 2020. Advanced Calculus: Theory and Practice, second ed. Chapman and Hall/CRC, New York, http://dx.doi.org/10.1201/9780203705148.

Pikal, M.J., Bogner, R., Mudhivarthi, V., Sharma, P., Sane, P., 2016. Freeze-drying process development and scale-up: Scale-up of edge vial versus center vial heat transfer coefficients, K_v. J. Pharm. Sci. 105 (11), 3333–3343. http://dx.doi.org/10.1016/j.xphs.2016.07.027.

Pikal, M.J., Mascarenhas, W.J., Akay, H.U., Cardon, S., Bhugra, C., Jameel, F., Rambhatla, S., 2005. The nonsteady state modeling of freeze drying: In-process product temperature and moisture content mapping and pharmaceutical product quality applications. Pharm. Dev. Technol. 10 (1), 17–32. http://dx.doi.org/10.1081/PDT-35869.

Pikal, M.J., Roy, M.L., Shah, S., 1984. Mass and heat transfer in vial freeze-drying of pharmaceuticals: Role of the vial. J. Pharm. Sci. 73 (9), 1224–1237. http://dx.doi.org/10.1002/jps.2600730910.

Pisano, R., Fissore, D., Velardi, S.A., Barresi, A.A., 2010. In-line optimization and control of an industrial freeze-drying process for pharmaceuticals. J. Pharm. Sci. 99 (11), 4691–4709. http://dx.doi.org/10.1002/jps.22166.

Scutellà, B., Plana-Fattori, A., Passot, S., Bourlès, E., Fonseca, F., Flick, D., Tréléa, I., 2017. 3D mathematical modelling to understand atypical heat transfer observed in vial freeze-drying. Appl. Therm. Eng. 126, 226–236. http://dx.doi.org/10.1016/j.applthermaleng.2017.07.096.

Strang, G., 2007. Computational Science and Engineering. Wellesley-Cambridge Press, Wellesley.

Taler, J., Duda, P., 2006. Solving Direct and Inverse Heat Conduction Problems. Springer, Berlin, Heidelberg, http://dx.doi.org/10.1007/978-3-540-33471-2_24.

Velardi, S.A., Barresi, A.A., 2008. Development of simplified models for the freeze-drying process and investigation of the optimal operating conditions. Chem. Eng. Res. Des. 86 (1), 9–22. http://dx.doi.org/10.1016/j.cherd.2007.10.007.

Walters, R.H., Bhatnagar, B., Tchessalov, S., Izutsu, K.-I., Tsumoto, K., Ohtake, S., 2014. Next generation drying technologies for pharmaceutical applications. J. Pharm. Sci. 103 (9), 2673–2695. http://dx.doi.org/10.1002/jps.23998.

Wang, W., Zhang, S., Pan, Y., Yang, J., Tang, Y., Chen, G., 2020. Multiphysics modeling for microwave freeze-drying of initially porous frozen material assisted by wave-absorptive medium. Ind. Eng. Chem. Res. 59 (47), 20903–20915. http://dx.doi.org/10.1021/acs.iecr.0c03852.

Wegiel, L.A., Ferris, S.J., Nail, S.L., 2018. Experimental aspects of measuring the vial heat transfer coefficient in pharmaceutical freeze-drying. AAPS PharmSciTech 19 (4), 1810–1817. http://dx.doi.org/10.1208/s12249-018-0998-z.

Witkiewicz, K., Nastaj, J.F., 2010. Simulation strategies in mathematical modeling of microwave heating in freeze-drying process. Dry. Technol. 28 (8), 1001–1012. http://dx.doi.org/10.1080/07373937.2010.497090.